AIP Journal of Applied Physics

Structural analysis of liquid aluminum at high pressure and high temperature using the hard sphere model

Daijo Ikuta, Yoshio Kono, and Guoyin Shen

Citation: Journal of Applied Physics **120**, 135901 (2016); doi: 10.1063/1.4963278
View online: http://dx.doi.org/10.1063/1.4963278
View Table of Contents: http://scitation.aip.org/content/aip/journal/jap/120/13?ver=pdfcov
Published by the AIP Publishing

Articles you may be interested in

Atomic study on the ordered structure in Al melts induced by liquid/substrate interface with Ti solute
Appl. Phys. Lett. **106**, 041606 (2015); 10.1063/1.4907171

Study of liquid gallium as a function of pressure and temperature using synchrotron x-ray microtomography and x-ray diffraction
Appl. Phys. Lett. **105**, 041906 (2014); 10.1063/1.4891572

Study of liquid gallium at high pressure using synchrotron x-ray
J. Appl. Phys. **111**, 112629 (2012); 10.1063/1.4726256

Polymorphism and metastable phenomena in liquid tin under pressure
Appl. Phys. Lett. **89**, 221912 (2006); 10.1063/1.2397568

Multichannel collimator for structural investigation of liquids and amorphous materials at high pressures and temperatures
Rev. Sci. Instrum. **73**, 3570 (2002); 10.1063/1.1505104

Reuse of AIP Publishing content is subject to the terms at: https://publishing.aip.org/authors/rights-and-permissions. Download to IP: 164.54.164.67 On: Mon, 03 Oct 2016 20:30:40

JOURNAL OF APPLIED PHYSICS **120**, 135901 (2016)

Structural analysis of liquid aluminum at high pressure and high temperature using the hard sphere model

Daijo Ikuta,[a] Yoshio Kono, and Guoyin Shen
High Pressure Collaborative Access Team, Geophysical Laboratory, Carnegie Institution of Washington, Argonne, Illinois 60439, USA

(Received 6 June 2016; accepted 10 September 2016; published online 3 October 2016)

The structure of liquid aluminum is measured up to 6.9 GPa and 1773 K using a multi-angle energy-dispersive X-ray diffraction method in a Paris-Edinburgh press. The effect of pressure and temperature on the structure and density of liquid aluminum is analyzed by means of the hard sphere model. Peak positions in the structure factor of liquid aluminum show a nearly constant value with varying temperatures at ∼1–2 GPa and slightly change with varying pressures up to 6.9 GPa at 1173–1773 K. In contrast, the height of the first peak in the structure factor significantly changes with varying pressures and temperatures. Hard sphere model analysis shows that the structure of liquid aluminum in the pressure-temperature range of this study is controlled mostly by the packing fraction with only a minor change in hard sphere diameters. The obtained packing fractions and hard sphere diameters are used to calculate densities of liquid aluminum at high pressure-temperature conditions. *Published by AIP Publishing.*
[http://dx.doi.org/10.1063/1.4963278]

I. INTRODUCTION

Liquid metals are traditionally classified into three types:[1] (I) the structure factor $S(Q)$ shows a simple symmetric wave form, (II) the first peak of the $S(Q)$ has a shoulder on the high-Q side, and (III) the first peak of the $S(Q)$ shows an asymmetry form. Liquid aluminum is a typical example of liquid metals of type-I. The so-called Al-type liquid metal contains aluminum, iron, magnesium, etc., and accounts for ∼80% of entire liquid metals.[1] Therefore, the study of structure and physical properties of liquid aluminum is of fundamental importance in understanding liquid metals.

The structure of liquid aluminum has been investigated by both experiment and theory at ambient pressure. Waseda[1] showed that the $S(Q)$ of liquid aluminum is close to a simple symmetric wave form which fits well into a single component system of the hard sphere model (HSM) by Ashcroft and Lekner.[2] Their results show that the packing fraction of liquid aluminum decreases from 0.45 to 0.39 with increasing temperature from 943 to 1323 K under ambient pressure. A density function theory study[3] also showed that the packing fraction of liquid aluminum linearly decreases from 0.466 to 0.415 and the coordination number of liquid aluminum decreases from 12.0 to 11.5 with increasing temperature from 875 to 1250 K. In addition, some efforts have been made to determine the physical properties of liquid aluminum. For example, the density of liquid aluminum has been studied at high temperatures under ambient pressure conditions by using several methods such as the X-ray attenuation technique,[4] volumetric method,[5] and large-drop method.[6,7] Nevertheless, the structure of liquid aluminum at high pressures has not been studied due to technical difficulties. Recently, efforts have been made to develop the structure measurement of liquids at high pressure and high temperature conditions using a Paris-Edinburgh (PE) press at the 16-BM-B beamline at the Advanced Photon Source,[8] and successful results for the structure of liquids at high pressure and high temperature conditions were demonstrated in some systems such as liquid metals,[9,10] molten salts,[11] carbonate melts,[12] and silicate melts.[13] In this study, we applied the recently developed technique to investigate the structure of liquid aluminum up to 6.9 GPa and 1773 K. The structural data provide the information of the effect of pressure and temperature on the structure and density of liquid aluminum by applying the hard sphere model analysis.

II. EXPERIMENTAL METHODS

A. High-pressure experiments

The structure of liquid aluminum was measured by *in situ* energy dispersive X-ray diffraction (EDXD) experiments at high pressures and high temperatures using a Paris-Edinburgh (PE) press[14] at the beamline 16-BM-B[8] at High Pressure Collaborative Access Team (HPCAT) at the Advanced Photon Source. We used a standard PE cell assembly,[8] which is mainly composed of boron-nitride sample capsule, MgO ring, graphite heater, boron-epoxy gaskets, and ZrO_2 caps. The sample is aluminum powder (99.5%, −325 mesh, Alfa Aesar), which is shaped into a cylinder with 1.5 mm diameter and 2 mm height by using a pellet die. Although the anvil gap becomes smaller than the sample height at high pressure conditions, more than 500 μm sample height was available for X-ray diffraction at high pressure-temperature (P-T) conditions. The X-ray radiography setup[8] was used to check capsulation of the liquid sample. We confirmed no change in the cylindrical sample shape during experiment, which indicates no leak of the liquid sample. High temperature was generated by using a graphite heater. Temperatures were estimated by the power-temperature curves

[a]E-mail: dikuta@carnegiescience.edu

Reuse of AIP Publishing content is subject to the terms at: https://publishing.aip.org/authors/rights-and-permissions. Download to IP: 164.54.164.67 On: Mon, 03 Oct 2016 20:30:40

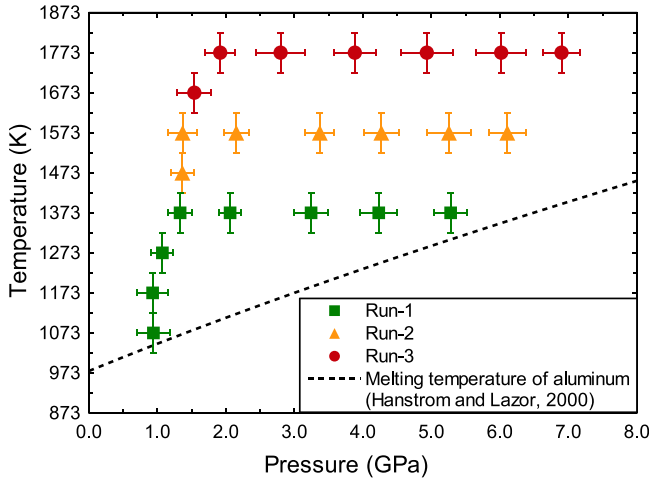

FIG. 1. The pressure and temperature conditions of this study. Errors in temperature are estimated to be less than 50 K by the reproducibility of melting curves of NaCl and KCl.[11] Overall errors in pressure are estimated to be less than 0.5 GPa that contains the differences of pressure before and after a structural measurement of about 0.3 GPa and experimental errors of about 0.1 GPa.

determined in a separate experiment using an identical cell assembly.[8] Uncertainty in temperature is estimated to be less than 50 K by the reproducibility of melting curves of NaCl and KCl.[11] Pressures are determined by using the equation of state of MgO.[15] The pressure measurement was conducted before and after the structure measurement and the average value is adopted. The pressure difference before and after the structure measurement was less than 0.5 GPa.

Figure 1 shows the experimental P-T conditions of this study. Run-1 was conducted isobarically at four temperatures of 1073, 1173, 1273, and 1373 K around 1 GPa and then isothermally at five pressures of 1.3, 2.1, 3.2 4.2, 5.3, and 4.6 GPa at 1373 K. In Run-2, the structure measurement was conducted at two temperatures of 1473 and 1573 K at 1.4 GPa and then isothermally at six pressures at 1.4, 2.2, 3.4, 4.3, 5.3, and 6.1 GPa at 1573 K. In Run-3, the structure measurement was conducted at two temperatures at 1673 K at 1.5 GPa and 1773 K at 1.9 GPa, and six isothermal pressures at 1.9, 2.8, 3.9, 4.9, 6.0, and 6.9 GPa at 1773 K.

B. Liquid structure measurements

Structure factor $S(Q)$ of liquid aluminum was measured by multi-angle EDXD using a Ge solid-state detector. EDXD patterns were collected at seven diffraction angles ($2\theta = 3.0$, 4.5, 6.0, 9.0, 12.0, 18.0, and 25.0°), until counts reached at least 1000 counts at a high energy (90 keV) at each 2θ angle. The total data acquisition time to obtain the seven EDXD patterns was 3.5 h. For background subtraction, background EDXD patterns at each 2θ angle were taken with the same exposure time and the slit set-up with an empty cell assembly which was composed of the identical cell parts without the sample.

Figure 2(a) shows an example of EDXD patterns at 6.9 GPa and 1773 K after background subtraction, with data binning to increase the signal-to-noise ratio and subtraction of crystalline peaks arising from the surrounding capsule material

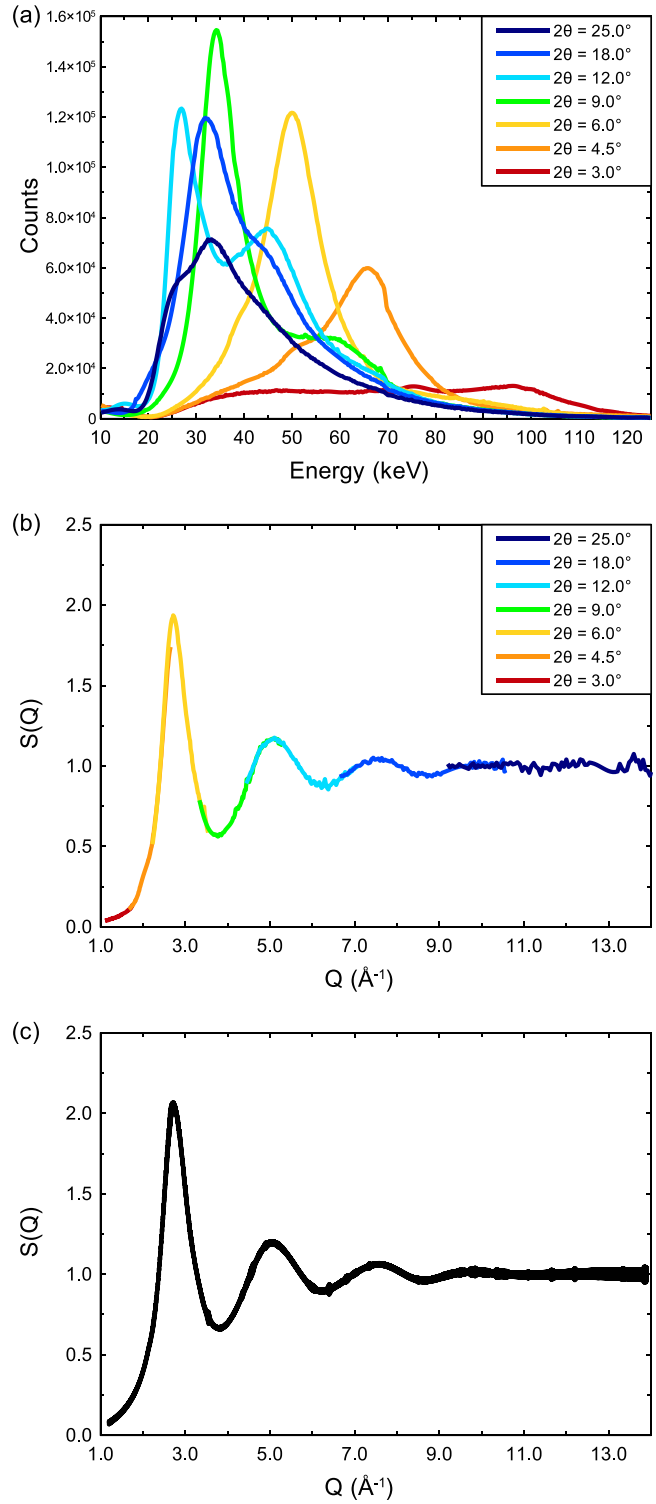

FIG. 2. (a) EDXD patterns at seven 2θ angles at 6.9 GPa and 1773 K after background subtraction, data binning, and subtraction of crystalline peaks from the surrounding capsule material (BN). (b) An example of the structure factor $S(Q)$ directly derived from the EDXD spectra in (a). (c) The $S(Q)$ after optimization[17] with the Kaplow-type correction.[16] Errors are indicated by the width of the lines.

(BN) particularly at low 2θ angles. The absorption at ~69 keV is tungsten absorption edge from beamline components such as tungsten slits. $S(Q)$ was derived from the EDXD patterns by using the program, aEDXD, developed by Park.[8] Figure 2(b) shows the structure factor at the momentum transfer Q-range up

Reuse of AIP Publishing content is subject to the terms at: https://publishing.aip.org/authors/rights-and-permissions. Download to IP: 164.54.164.67 On: Mon, 03 Oct 2016 20:30:40

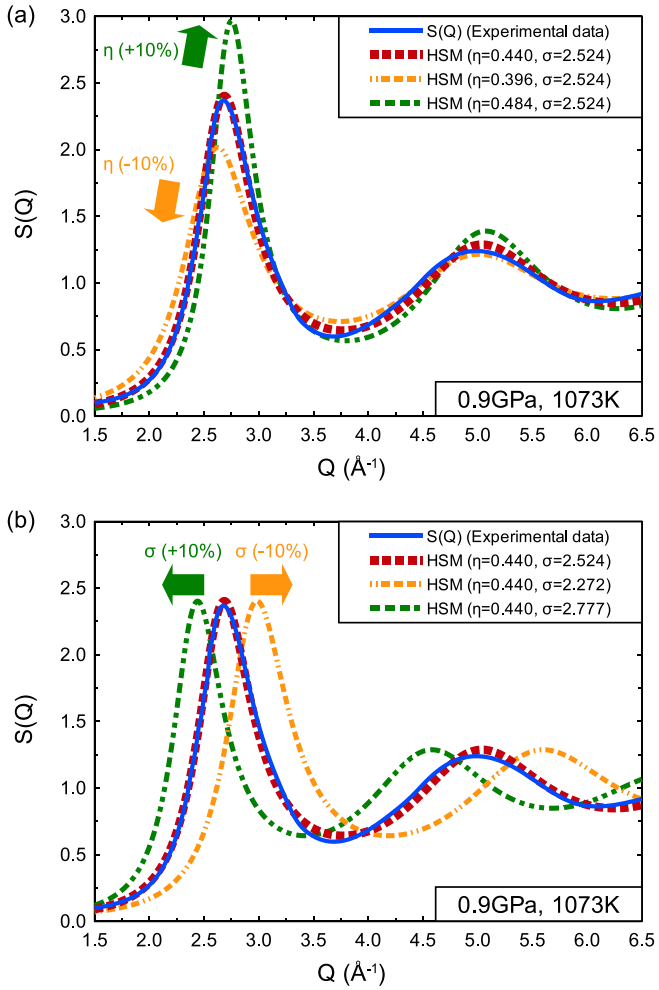

FIG. 3. Examples of the HSM fitting to $S(Q)$. The blue solid line represents experimentally obtained $S(Q)$ at 0.9 GPa and 1073 K, and dashed red line represents the HSM fitting result. (a) Influence of the packing density on $S(Q)$. Green and yellow dashed lines show $S(Q)$ calculated by using 10% higher and lower values of the packing density, respectively. (b) Influence of the hard sphere diameter on $S(Q)$. Green and yellow dashed lines show $S(Q)$ calculated by using 10% higher and lower values of the hard sphere diameter, respectively.

to 14 $Å^{-1}$, obtained by analyzing the EDXD patterns shown in Fig. 2(a). The Kaplow-type correction[16] and an optimization method[17] were applied in determining final $S(Q)$ (Fig. 2(c)). The optimization process was iterated five times. To apply the optimization process, the number density of liquid aluminum is required. At first, we derived a temporary $S(Q)$ by using a constant value of the number density (0.0531 atom/$Å^3$), an average value of previous studies at ambient pressure just above melting temperature.[18] We then optimized the number density from the temporary $S(Q)$ using the HSM analysis as described in Section III. We repeated the optimization process using the obtained number density and finally determined the optimal $S(Q)$ results.

III. THE HARD SPHERE MODEL APPROACH

The HSM has been widely used as a basic theory for understanding gases and liquids (e.g., Ref. 1). The hard sphere system is defined as a collection randomly filled with undeformable hard spheres without overlapping. This filling theory was proposed by Ornstein and Zernike[19] and has been

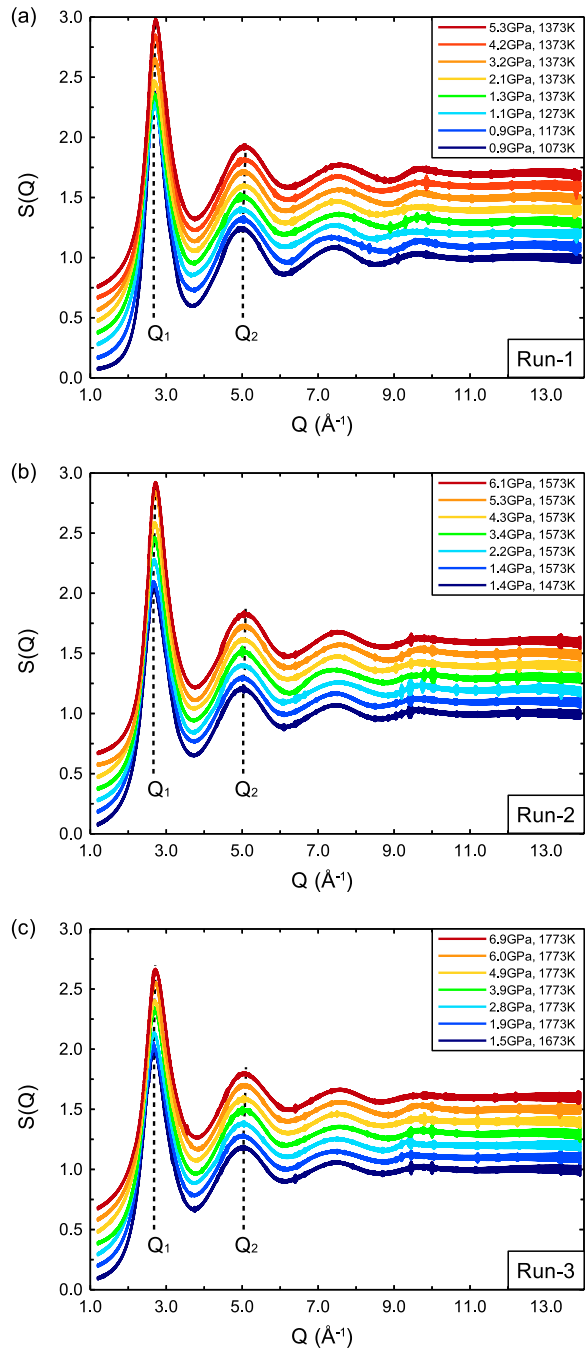

FIG. 4. Structure factors $S(Q)$ of liquid aluminum. $S(Q)$ is shown by an offset of 0.1 in the vertical axis for clarity. The line width indicated the errors of $S(Q)$. Black dashed lines indicate the first (Q_1) and second (Q_2) peak positions, respectively.

used with some additional approximation such as Percus-Yevick approximation.[20] Several types of the HSM with Percus-Yevick approximation were proposed to model liquid metals (e.g., Refs. 21–24). According to previous ambient pressure studies (e.g., Ref. 1), $S(Q)$ of simple liquid metals such as liquid aluminum can be well reproduced by the HSM of the single component system proposed by Ashcroft and Lekner.[2] We therefore applied the HSM model proposed by Ashcroft and Lekner[2] to analyze our data at high P-T. The structure factor $S(Q)$ in the HSM can be described by the following equations:[2]

Reuse of AIP Publishing content is subject to the terms at: https://publishing.aip.org/authors/rights-and-permissions. Download to IP: 164.54.164.67 On: Mon, 03 Oct 2016 20:30:40

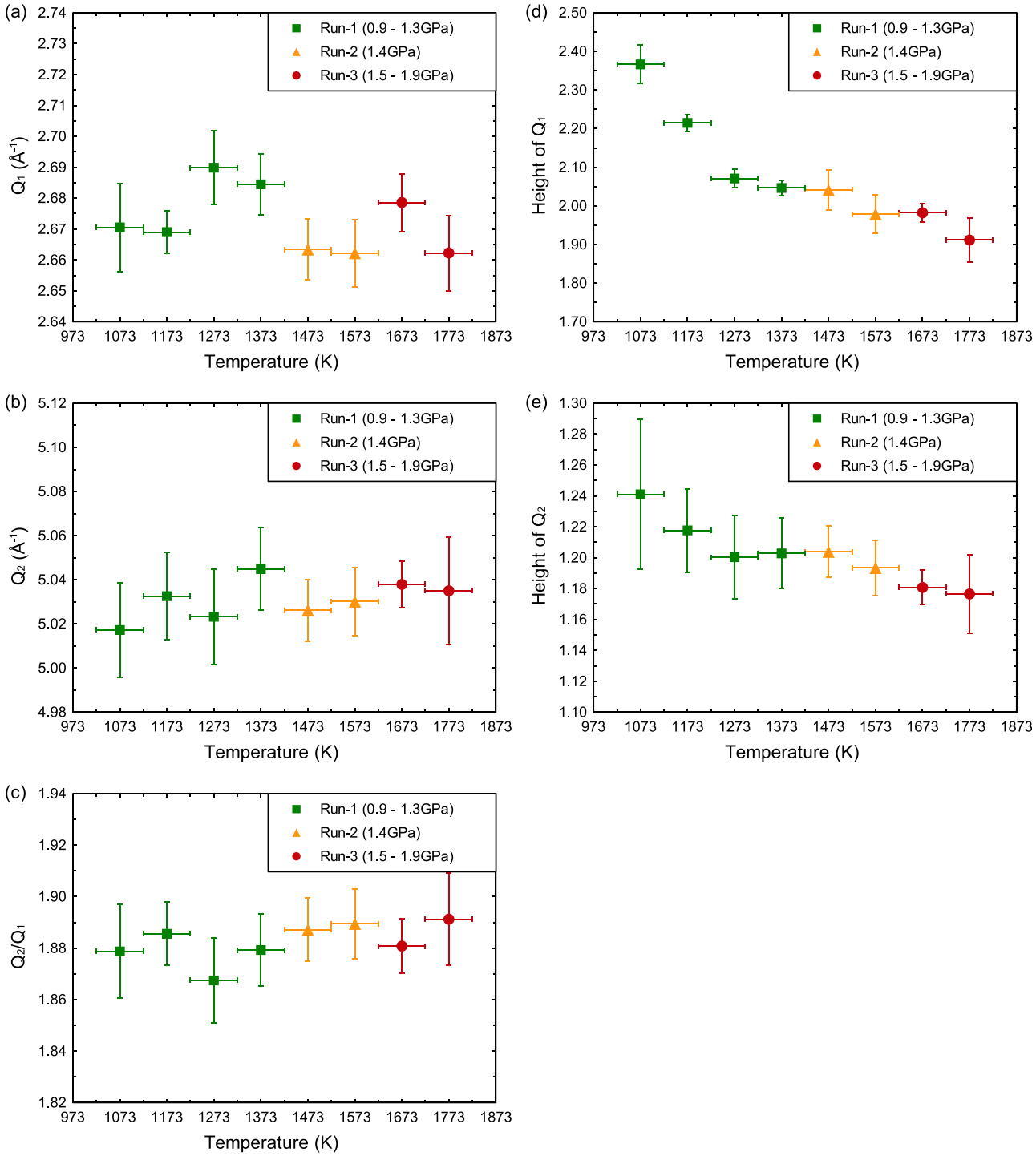

FIG. 5. Temperature dependences of the first and second peak positions and heights of liquid aluminum. Abbreviation: Q_1 = the first peak position as shown in Fig. 4, Q_2 = the second peak position as marked in Fig. 4, Q_2/Q_1 = ratio of the first and second peak positions. For the errors of both peak positions, statistical errors from the uncertainties in $S(Q)$ are very small, and thus overall errors with fitting errors in peak position determination are less than 0.5%. In the height of Q_1 determination, statistical errors from the uncertainties in $S(Q)$ are less than 1% and fitting errors are less than 0.5%–1%. Thus, overall errors in the height of Q_1 determination are estimated to be less than 2%. In the height of Q_2 determination, statistical errors from the uncertainties in $S(Q)$ are about 1%–1.5% and fitting errors are ~1%–1.5%. Thus, overall errors in the height of Q_2 determination are estimated to be ~3%.

$$S(Q\sigma) = \frac{1}{1 - \rho_N c(Q\sigma)}, \tag{1}$$

$$c(Q\sigma) = -4\pi\sigma^3 \int_0^1 s^2 \frac{\sin(sQ\sigma)}{sQ\sigma} \left(\alpha + \beta s + \gamma s^3\right) ds, \tag{2}$$

$$\alpha = \frac{(1+2\eta)^2}{(1-\eta)^4}, \quad \beta = -6\eta\frac{(1+\eta/2)^2}{(1-\eta)^4}, \quad \gamma = \frac{\eta}{2}\frac{(1+2\eta)^2}{(1-4\eta)^4}, \tag{3}$$

$$\rho_N = \frac{6\eta}{\pi\sigma^3}, \tag{4}$$

where $c(Q\sigma)$ is the direct correlation function that is transformed to bipolar coordinates and is integrated over the angular variable s, η is the packing fraction, and σ is the hard sphere diameter. Number density (ρ_N) is correlated with the

Reuse of AIP Publishing content is subject to the terms at: https://publishing.aip.org/authors/rights-and-permissions. Download to IP: 164.54.164.67 On: Mon, 03 Oct 2016 20:30:40

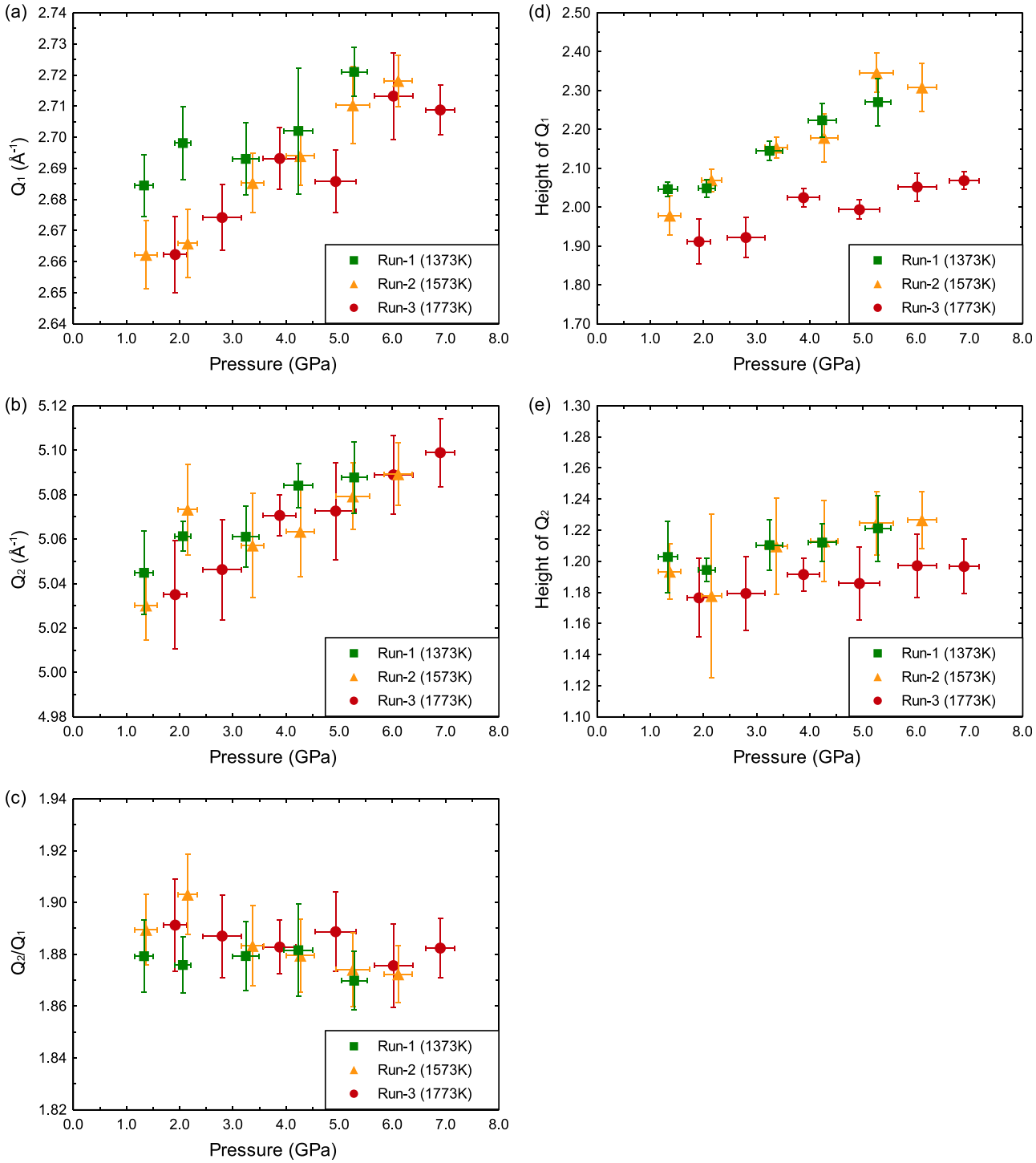

FIG. 6. Pressure dependences of the first and second peak positions and heights of liquid aluminum. For the errors of both peak positions, statistical errors from the uncertainties in $S(Q)$ are very small; thus, overall errors with fitting errors in peak position determination are less than 0.5%. In the height of Q_1 determination, statistical errors from the uncertainties in $S(Q)$ are less than 1% and fitting errors are less than 0.5%–1%. Thus, the overall errors in the height of Q_1 determination are estimated to be less than 2%. In the height of Q_2 determination, statistical errors from the uncertainties in $S(Q)$ are about 1%–1.5% and fitting errors are ~1%–1.5%. Thus, overall errors in the height of Q_2 determination are estimated to be ~3%.

packing fraction and hard sphere diameter (Eq. (4)), and therefore the HSM can be described by two free parameters of the packing fraction and hard sphere diameter. In this study, we applied the model to obtain both the packing fraction and the hard sphere diameter. Thus, the number density can be derived from experimentally measured $S(Q)$ at high pressures and high temperatures.

Figure 3 shows an example of the effect of packing fraction and hard sphere diameter on $S(Q)$ by the HSM analysis. In the HSM,[2] increasing packing fraction enhances intensity of peaks, sharpens the peak shape, and shifts the peak position to the high-Q side (Fig. 3(a)), while the variation of the hard sphere diameter influences mostly on the peak position (Fig. 3(b)).

Reuse of AIP Publishing content is subject to the terms at: https://publishing.aip.org/authors/rights-and-permissions. Download to IP: 164.54.164.67 On: Mon, 03 Oct 2016 20:30:40

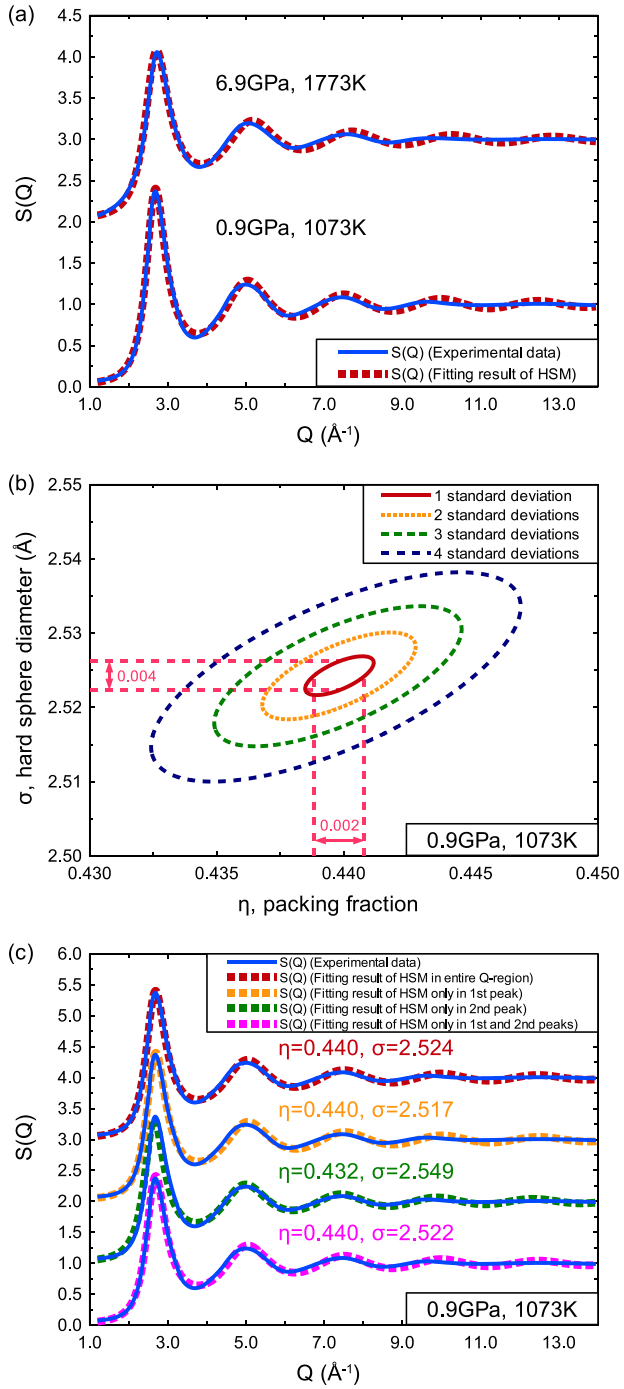

FIG. 7. Examples of the HSM fitting to $S(Q)$. (a) Typical fitting results of the HSM applied to the experimental results at 0.9 GPa and 1073 K and at 6.9 GPa and 1773 K. The blue solid line represents experimentally obtained $S(Q)$, and the dashed red line represents the HSM fitting result. (b) Contour plot of the error analysis of HSM model fitting. The red solid line, yellow dotted line, green dashed line, and blue dashed line represent 1, 2, 3, and 4 standard deviation(s). (c) Typical result of HSM model fitting with the limited Q-region. The blue solid line represents experimentally obtained $S(Q)$. Dashed red, yellow, green, and magenta lines represent the HSM fitting result with fitting in the entire Q-region, only in the first sharp peak, only in the second sharp peak, and only in the first and second sharp peaks, respectively.

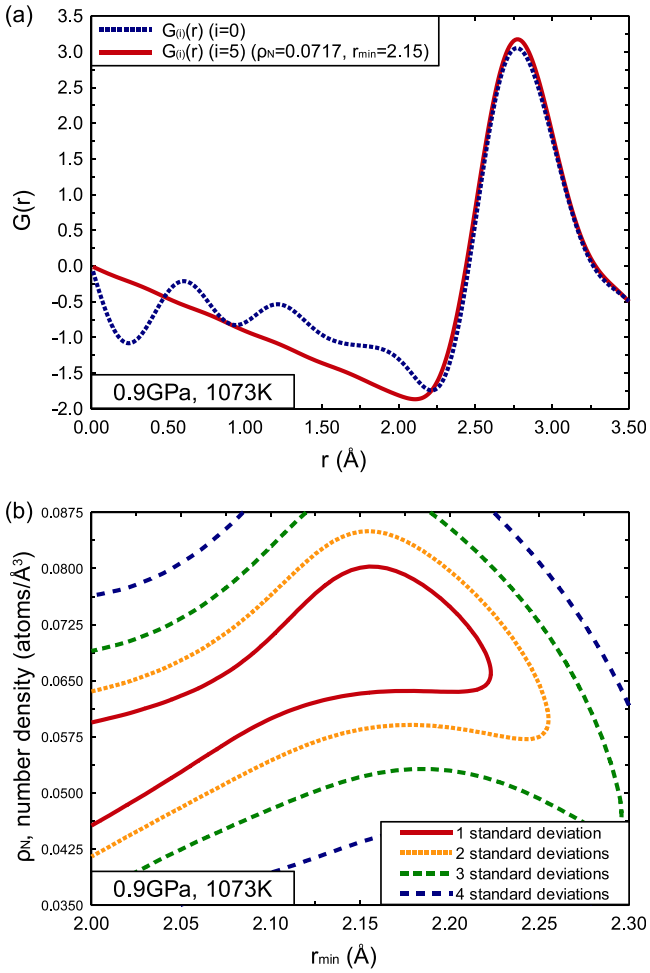

FIG. 8. Example of applying Eggert's method.[26] (a) The distribution function $G_{(i)}(r)$ after i-times optimization procedure. The blue dotted line represents $G_{(0)}(r)$ before optimization and the red solid line represents $G_{(5)}(r)$ after five times optimization. (b) Contour plot of the error analysis of Eggert's method. The red solid line, yellow dotted line, green dashed line, and blue dashed line represent 1, 2, 3, and 4 standard deviation(s).

IV. RESULTS AND DISCUSSION

Figure 4 shows structure factors $S(Q)$ at high P-T obtained in the three runs. We determined $S(Q)$ at Q-range up to 14 Å^{-1}. The line widths of $S(Q)$ indicate the uncertainties in intensity. Our results show very small errors in intensity especially at low-Q range (Fig. 4). All $S(Q)$ show oscillation around 1. Three oscillations are clearly visible at Q-range less than ~9 Å^{-1}, and weak forth oscillation can be seen at Q-range at ~9–11 Å^{-1}. These facts indicate the high quality of our $S(Q)$ results, similar to those obtained at ambient pressure.[25] The high quality $S(Q)$ data allow us to precisely fit $S(Q)$ by using the HSM to determine the packing fraction and the hard sphere diameter and the resultant density.

Figure 5 shows the temperature dependences of the first and second peak positions and their heights. We observed almost constant positions of the first (Q_1) and second (Q_2) peaks of $S(Q)$ with varying temperatures under ~1–2 GPa (Figs. 5(a) and 5(b)). We observed $Q_1 = \sim 2.67$ Å^{-1}, $Q_2 = \sim 5.03$ Å^{-1}, and the ratio $Q_2/Q_1 = \sim 1.88$ up to 1773 K under ~1–2 GPa with the variation of less than 1%. The constant peak positions of the Q_1 and Q_2 of $S(Q)$ are consistent with the previous result at ambient pressure.[25] On the other hand, the heights of the first and second peaks clearly decrease with increasing temperature (Figs. 5(d) and 5(e)),

Reuse of AIP Publishing content is subject to the terms at: https://publishing.aip.org/authors/rights-and-permissions. Download to IP: 164.54.164.67 On: Mon, 03 Oct 2016 20:30:40

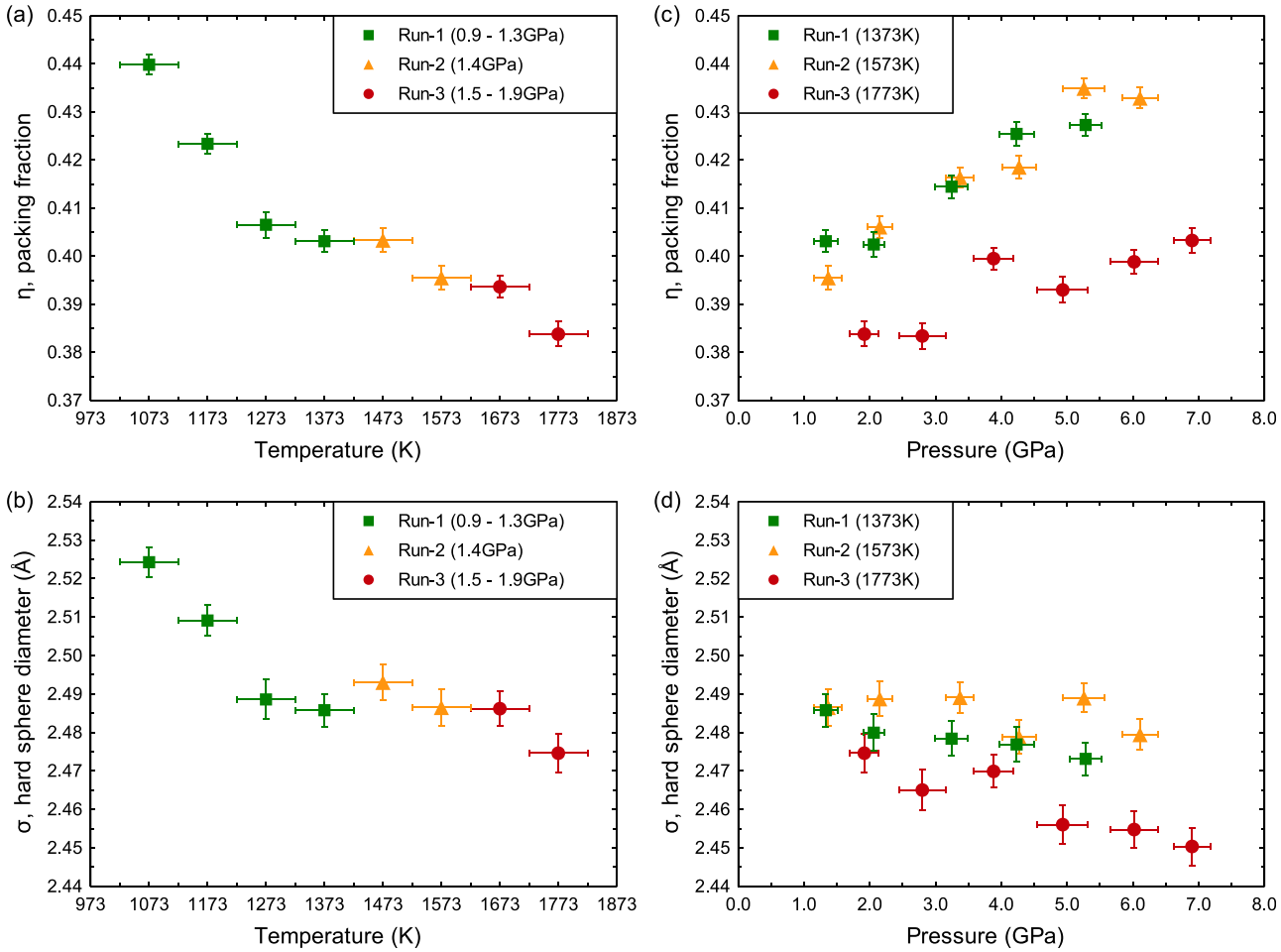

FIG. 9. Packing fraction and hard sphere diameter of liquid aluminum. (a) and (b) show temperature dependences of the packing fraction and the hard sphere diameter, respectively. (c) and (d) show pressure dependences of the packing fraction and the hard sphere diameter, respectively.

which is also similar to the results of the previous ambient pressure study.[25] Figure 6 shows pressure dependences of the Q_1 and Q_2 positions, Q_2/Q_1 ratio, and heights of the first and second peaks at 1373, 1573, and 1773 K. Both Q_1 and Q_2 positions increase by up to 2.1% and 1.3%, respectively, with increasing pressure, while the Q_2/Q_1 ratio is almost constant within the errors. The height of the first peak markedly increases by up to 13.4% with increasing pressure. Although the height of the second peak changes by up to 4.1%, the data are scattered within the experimental errors.

We fit the obtained $S(Q)$ results into the HSM model. Typical fitting results of $S(Q)$ with the HSM model are shown in Fig. 7(a). Figure 7(b) shows the error analysis of the HSM fitting for the data at 0.9 GPa and 1073 K. We obtain the packing fraction $\eta = 0.440$ and the hard sphere diameter $\sigma = 2.524$ Å with the 1 standard deviation errors of ± 0.002 for the packing fraction and ± 0.004 for the hard sphere diameter. The resultant density ρ is 2.34 ± 0.02 (g/cm^3).

We find slight inconsistency in the peak positions between the first and second peaks in the HSM results (Fig. 7(a)). The HSM results show the second peak position at slightly higher-Q side and higher height in comparison with experimental results (Fig. 7(a)). The differences of the position and the height of the second peak between experimental and HSM results are 0.4% and 3.7% at 0.9 GPa and 1073 K, respectively, and 1.2% and 2.3% at 6.9 GPa and 1773 K, respectively. To evaluate the effect of the peak position difference by the different peaks on the HSM model results, we did test analysis using limited Q-range for the HSM analysis. Figure 7(c) shows the HSM analysis results by using different Q-ranges. HSM fitting with only the first peak region ($Q = 1.2$–3.69 Å) gives the parameters $\eta = 0.440$, $\sigma = 2.517$ Å, and $\rho = 2.36$ g/cm^3. The difference in the packing fraction and hard sphere diameter between the fitting in the entire Q-range and the fitting only in the first peak is 0.03% and 0.30%, respectively, and the resultant difference in density is 0.86%. The HSM fitting only using the second peak ($Q = 3.69$–6.09 Å^{-1}) gives the parameters $\eta = 0.432$, $\sigma = 2.549$ Å, and $\rho = 2.24$ g/cm^3, which is 1.70%, 0.96%, and 4.48% different from that obtained from the fitting in the entire Q-range, respectively. On the other hand, the HSM fitting using both the first and second peaks gives the parameters $\eta = 0.440$, $\sigma = 2.522$ Å, and $\rho = 2.35$ g/cm^3, which is almost the same as that obtained by the fitting in the entire Q-range (0.15%, 0.07%, and 0.36% difference, respectively). This result indicates that combination of the first and second peaks of the $S(Q)$ may represent the structure of liquid aluminum.

Some previous studies[26–28] have used the pair distribution function $G(r)$ to obtain density. In the method proposed

Reuse of AIP Publishing content is subject to the terms at: https://publishing.aip.org/authors/rights-and-permissions. Download to IP: 164.54.164.67 On: Mon, 03 Oct 2016 20:30:40

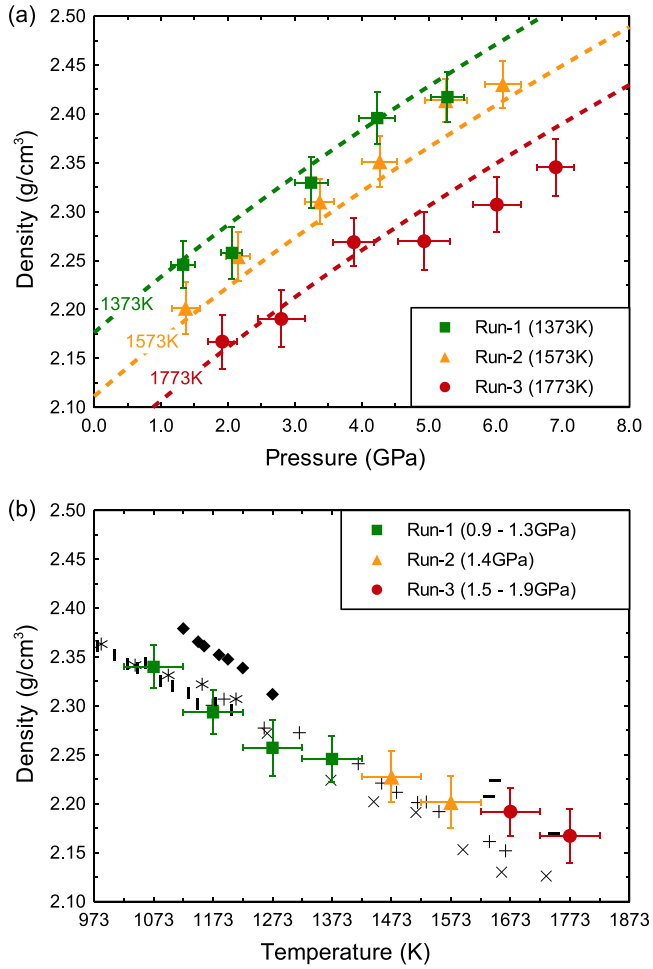

FIG. 10. Density of liquid aluminum as a function of pressure and temperature. (a) Density of liquid aluminum as a function of pressure at 1373, 1573, and 1773 K. The dashed line represents the results of high-temperature 2nd-order Birch-Murnaghan equation of state fitting (Table II). In the density determination, statistical errors from the uncertainties in $S(Q)$ are up to 1%. In addition, fitting errors of each parameter in the HSM are less than 0.5–1% (Table I). Thus, overall errors in density determination are estimated to be less than 2%. (b) Temperature dependences of the density of liquid aluminum. Our experimental data (color solid symbols) were obtained at 0.9–1.9 GPa from three runs. Black symbols show density data determined at ambient pressure (pluses: Levin *et al.*,[6] crosses: Gol'tsova,[5] asterisks: Smith *et al.*,[4] vertical bars: Yatsenko *et al.*,[7] horizontal bars: Hanstrom and Lazor,[31] and diamonds: Mauro *et al.*[25]).

by Eggert *et al.*,[26] the density is derived from a small r-region of the $G(r)$ by assuming that atoms cannot exist within atomic core diameter r_{min}, and $G(r)$ in the r-region smaller than r_{min} should be expressed by $-4\pi r\rho_N$. Therefore, the density can be calculated by optimizing $G(r)$ at r smaller than r_{min}. We also attempted to apply the method to our liquid aluminum data obtained at 0.9 GPa and 1073 K to compare the analysis result with the HSM model. The initial $G(r)$ ($G_{(0)}(r)$) has large oscillations in the small-r region (Fig. 8(a)). We conducted the five-times iterative optimization process[17] to minimize the unphysical oscillations, and the obtained $G(r)$ ($G_{(5)}(r)$) after five times optimization procedure shows small oscillations at r range smaller than r_{min} (Fig. 8(a)). Figure 8(b) shows the uncertainty map as functions of two parameters of r_{min} and density obtained through the Eggert's density analysis. We find strong correlation between density and r_{min} in the error distribution. The results show that the final result with the minimum uncertainty strongly depends on the shape of initial oscillation in $G_{(0)}(r)$. Fitting of our liquid aluminum data into the Eggert's method[26] shows that the density value can vary by >10% with varying r_{min} within 1 standard deviation error. These tests do not support the use of the Eggert's method to determine density from our obtained data. Eggert's analysis may be used only when the initial oscillations in $G_{(0)}(r)$ are small enough to avoid the strong dependence of the initial oscillation state on density derivation. Alternatively, the influence of the initial oscillation on density determination may be reduced by adopting another modification process in the experimental background as Eggert *et al.*[26] and Morard *et al.*[28] conducted. However, any modification of experimental data needs to be carefully validated. Since the HSM model analysis does not show such inter-dependence in the error analysis (Fig. 7(b)), we consider that the HSM analysis is a direct method for deriving density of type-I liquid metals such as liquid aluminum.

Figure 9 shows the temperature and pressure dependences of the packing fraction and the hard sphere diameter. With increasing temperature at 0.9–1.9 GPa, we observed decreases of both packing fraction and hard sphere diameter. The packing fraction decreases by 13% from 1073 to 1773 K, which is attributed to the strong decrease of heights of Q_1 and Q_2 peaks with increasing temperature (Figs. 5(d) and 5(e)). A previous experimental study[1] reported 12% decrease of packing fraction of liquid aluminum from 943 to 1323 K at ambient pressure, which is consistent with our results at 0.9–1.9 GPa. A theoretical study[3] also reported a strong decrease (11% decreases from 875 to 1250 K) of the packing fraction of liquid aluminum with increasing temperature at ambient pressure without significant change of hard sphere diameter. Similarly to liquid aluminum, some other simple liquid metals also show similar structural behavior with varying temperatures at ambient pressure. For example, the packing fraction of liquid indium decreases by 15% at the temperature range between 433 and 973 K at ambient pressure.[1] The packing fraction of liquid lead decreases by 31% at the temperature range between 613 and 1323 K at ambient pressure.[1] On the other hand, the hard sphere diameter shows relatively small change of less than 2%, due to small variation in the Q_1 and Q_2 positions with varying temperatures (Figs. 5(a) and 5(b)). The small change of the hard sphere diameter with varying temperatures is also consistent with the theoretical observations by Jakse and Pasturel.[3] Figures 9(c) and 9(d) show pressure dependences of the packing fraction and the hard sphere diameter, respectively. With increasing pressure from 1.3 to 6.9 GPa, the packing fraction gradually increases by up to 9%, while the hard sphere diameter showed slight decrease by less than 2%, because the shifts of the Q_1 and Q_2 positions with increasing pressure (Figs. 6(a) and 6(b)) are only up to 2.1%, which are markedly smaller than the change of the height of the Q_1 and Q_2 peaks of up to 17% (Figs. 6(d) and 6(e)). These data suggest that the structural change of liquid aluminum in the P-T range of this study is mainly controlled by the packing fraction.

Reuse of AIP Publishing content is subject to the terms at: https://publishing.aip.org/authors/rights-and-permissions. Download to IP: 164.54.164.67 On: Mon, 03 Oct 2016 20:30:40

TABLE I. Experimental conditions and structural results of liquid aluminum. Abbreviation: Q_1 = first peak position (Å^{-1}), Q_2 = second peak position (Å^{-1}), Q_2/Q_1 = ratio of the first and second peak positions, η = packing fraction, σ = hard sphere diameter (Å), and ρ = density (g/cm^3).

		Structure factor					Hard sphere model		
P (GPa)	T (K)	Q_1 (Å^{-1})	Q_2 (Å^{-1})	Height of Q_1	Height of Q_2	Q_2/Q_1	η	σ (Å)	ρ (g/cm^3)
0.9(2)	1073	2.67(1)	5.02(2)	2.37(5)	1.24(5)	1.88(2)	0.440(2)	2.524(4)	2.34(2)
0.9(2)	1173	2.67(1)	5.03(2)	2.21(2)	1.22(3)	1.89(1)	0.423(2)	2.509(4)	2.29(2)
1.1(2)	1273	2.69(1)	5.02(2)	2.07(2)	1.20(3)	1.87(2)	0.407(3)	2.489(5)	2.26(3)
1.3(2)	1373	2.68(1)	5.04(2)	2.05(2)	1.20(2)	1.88(1)	0.403(2)	2.486(4)	2.25(2)
2.1(2)	1373	2.70(1)	5.06(1)	2.05(2)	1.19(1)	1.88(1)	0.402(2)	2.480(5)	2.26(3)
3.2(2)	1373	2.69(1)	5.06(1)	2.15(2)	1.21(2)	1.88(1)	0.414(2)	2.478(4)	2.33(3)
4.2(3)	1373	2.70(2)	5.08(1)	2.22(4)	1.21(1)	1.88(2)	0.425(2)	2.477(4)	2.40(3)
5.3(2)	1373	2.72(1)	5.09(2)	2.27(6)	1.22(2)	1.87(1)	0.427(2)	2.473(4)	2.42(3)
1.4(2)	1473	2.66(1)	5.03(1)	2.04(5)	1.20(2)	1.89(1)	0.403(2)	2.493(5)	2.23(3)
1.4(2)	1573	2.66(1)	5.03(2)	1.98(5)	1.19(2)	1.89(1)	0.396(3)	2.486(5)	2.20(3)
2.2(2)	1573	2.67(1)	5.07(2)	2.07(3)	1.18(5)	1.90(2)	0.406(2)	2.489(4)	2.25(2)
3.4(2)	1573	2.69(1)	5.06(2)	2.15(3)	1.21(3)	1.88(2)	0.416(2)	2.489(4)	2.31(2)
4.3(3)	1573	2.69(1)	5.06(2)	2.18(6)	1.21(3)	1.88(1)	0.419(2)	2.479(4)	2.35(3)
5.3(3)	1573	2.71(1)	5.08(2)	2.35(5)	1.22(2)	1.87(1)	0.435(2)	2.489(4)	2.41(2)
6.1(3)	1573	2.72(1)	5.09(1)	2.31(6)	1.23(2)	1.87(1)	0.433(2)	2.479(4)	2.43(2)
1.5(2)	1673	2.68(1)	5.04(1)	1.98(2)	1.18(1)	1.88(1)	0.394(2)	2.486(4)	2.19(2)
1.9(2)	1773	2.66(1)	5.03(2)	1.91(6)	1.18(3)	1.89(2)	0.384(3)	2.475(5)	2.17(3)
2.8(4)	1773	2.67(1)	5.05(2)	1.92(5)	1.18(2)	1.89(2)	0.383(3)	2.465(5)	2.19(3)
3.9(3)	1773	2.69(1)	5.07(1)	2.02(2)	1.19(1)	1.88(1)	0.399(2)	2.470(4)	2.27(2)
4.9(4)	1773	2.69(1)	5.07(2)	1.99(2)	1.19(2)	1.89(2)	0.393(3)	2.456(5)	2.27(3)
6.0(4)	1773	2.71(1)	5.09(2)	2.05(4)	1.20(2)	1.88(2)	0.399(3)	2.455(5)	2.31(3)
6.9(3)	1773	2.71(1)	5.10(2)	2.07(2)	1.20(2)	1.88(1)	0.403(3)	2.450(5)	2.35(3)

Figure 10 shows the density of liquid aluminum at high P-T, calculated from the obtained packing fractions and hard sphere diameters (Eq. (4)). To represent our data, the density results are fitted into an equation similar to the high-temperature 2nd-order Birch-Murnaghan equation of state

$$P = \frac{3K}{2}\left[\left(\frac{\rho}{\rho_0}\right)^{\frac{7}{3}} - \left(\frac{\rho}{\rho_0}\right)^{\frac{5}{3}}\right], \tag{5}$$

$$\rho_0 = \rho_{0(T_0)} \times e^{-\alpha_0(T-T_0)}, \tag{6}$$

$$K = K_0 + (T - T_0)\left(\frac{dK}{dT}\right)_P. \tag{7}$$

Please note that, although the parameters K, dK/dT, and α_0 are considered as the bulk modulus, temperature dependence of the bulk modulus, and thermal expansion coefficient in the Birch-Murnaghan equation of state, we treat them as a set of fitted parameters that represent our results. Cautions need to be used when relating these parameters to their physical meanings. Other techniques such as the ultrasonic measurement (e.g., Ref. 29) may be used to further constrain the bulk modulus. The reference temperature (T_0) of 933.47 K is fixed at the melting temperature at ambient pressure.[30] We obtain density at the T_0 ($\rho_{0(T(0))} = 2.33 \pm 0.02$ g/cm^3), with fitted parameters of $K_0 = 40.44 \pm 4.39$ GPa, $\alpha_0 = 15.21 \times 10^{-5} \pm 1.92 \times 10^{-5}$ K^{-1}, and $dK/dT = -0.009 \pm 0.002$ GPa/K (Fig. 10(a) and Table II).

TABLE II. Parameters of the 2nd-order Birch-Murnaghan equations of state for liquid aluminum.

2nd-order Birch-Murnaghan	
T_0 (K)	933.47 (fixed)
ρ_0 (g/cm^3)	2.33 ± 0.02
K_0 (GPa)	40.44 ± 4.39
α_0 ($\times 10^{-5}$ (K^{-1}))	15.21 ± 1.92
dK/dT	-0.009 ± 0.002

Temperature dependence of the density obtained in this study at 0.9–1.9 GPa is compared with literature data at ambient pressure[4–7,25,31] (Fig. 10(b)). Gol'tsova,[5] Levin *et al.*,[6] Yatsenko *et al.*,[7] and Smith *et al.*[4] show similar density values, but Mauro *et al.*[25] and Hanstrom and Lazor[31] reported about 3% larger density than other studies. Our density data obtained at 0.9–1.9 GPa show almost similar values to those at ambient pressure in previous studies.[4–7,25,31] Calculated densities at ambient pressure by the fitted equation are 2.18, 2.11, and 2.05 (g/cm^3) at 1373, 1573, and 1773 K, respectively, which are ~3%–4% lower than the results of previous ambient pressure studies[4–7] at 1373, 1573, and 1773 K (2.25, 2.19, and 2.13 (g/cm^3), respectively). On the other hand, the slope of the temperature dependence of density obtained from our high pressure data is in good agreement with those of previous studies at ambient pressure.

V. CONCLUDING REMARKS

In this paper, we have investigated the structure and density of liquid aluminum using the experimentally determined structure factors combined with the HSM analysis. This method is useful not only for liquid aluminum but also for other type-I simple liquid metals such as liquid iron,

Reuse of AIP Publishing content is subject to the terms at: https://publishing.aip.org/authors/rights-and-permissions. Download to IP: 164.54.164.67 On: Mon, 03 Oct 2016 20:30:40

copper, and so on to understand the structure and density change with varying pressures and/or temperatures. Several hard sphere models have been proposed to express other types of liquid metals and/or two element systems such as the double hard sphere model (e.g., Refs. 21–24). Extension of the hard sphere model analysis to the double-hard sphere model should provide a plausible means to study the structure and density of other liquid metals and/or binary compositions.

We note a possible uncertainty due to possible interaction and overlapping of spheres for the determination of density of liquid metals by using the hard sphere model. For the hard sphere system, the mean nearest-neighbor distance between spheres becomes equal to the diameter of the hard sphere when the packing fraction reaches random close packing (0.64: e.g., Ref. 32),[33] and all hard spheres interact with each other. On the other hand, if spheres are soft, the mean nearest-neighbor distance can be shorter than the diameter of hard spheres, and density may become larger than that of the hard sphere with the same packing fraction. For example, if all soft spheres are randomly overlapped, the relationship among number density, packing fraction, and hard sphere diameter for the overlapping sphere is expressed by the following equation:[33]

$$\rho_N = \frac{-6\ln(1-\eta)}{\pi\sigma^3}. \tag{8}$$

This equation implies that, if all spheres are soft and they randomly overlap each other, the density of liquid may be ~25%–30% larger than that calculated based on the hard sphere model. Since our obtained packing fraction of liquid aluminum of 0.38–0.44 (Table I) is markedly smaller than the random close packing (0.64), we assume no overlapping of hard spheres in liquid aluminum at the pressure and temperature conditions of this study. On the other hand, if pressure increases to higher pressures, spheres may start overlapping, and the overlapping of spheres may influence on determination of density by the hard sphere model.

ACKNOWLEDGMENTS

This research was supported by DOE DE-FG02-99ER45775 and DE-NA0001974. We thank Curtis Kenney-Benson for his help in experiment and Changyong Park for his help in the aEDXD program. This work was performed at HPCAT, Sector 16, Advanced Photon Source, Argonne National Laboratory. HPCAT operations are supported by DOE-NNSA under Award No. DE-NA0001974 and DOE-BES under Award No. DE-FG02-99ER45775, with partial instrumentation funding by NSF. The Advanced Photon Source is a U.S. DOE Office of Science User Facility operated for the DOE Office of Science by Argonne National Laboratory under Contract No. DE-AC02-06CH11357. The PE press program is partly supported by GSECARS, which is supported by the NSF-EAR (EAR-1128799) and DOE-GeoSciences (DE-FG02-94ER14466).

[1]Y. Waseda, *The Structure of Non*-Crystalline *Materials*: *Liquids and Amorphous Solids* (McGraw-Hill International Book Co., New York, 1980).
[2]N. W. Ashcroft and J. Lekner, Phys. Rev. **145**, 83 (1966).
[3]N. Jakse and A. Pasturel, Sci. Rep. **3**, 3135 (2013).
[4]P. M. Smith, J. W. Elmer, and G. F. Gallegos, Scr. Mater. **40**, 937 (1999).
[5]E. I. Gol'tsova, High Temp. **3**, 438 (1965).
[6]E. S. Levin, G. D. Ayushina, and P. V. Gel'd, High Temp. **6**, 416 (1968).
[7]S. P. Yatsenko, V. I. Kononenko, and A. L. Sukhman, High Temp. **10**, 55 (1972).
[8]Y. Kono, C. Park, C. Kenney-Benson, G. Shen, and Y. Wang, Phys. Earth Planet. Inter. **228**, 269 (2014).
[9]Y. Kono, C. Kenney-Benson, Y. Shibazaki, C. Park, G. Shen, and Y. Wang, Phys. Earth Planet. Inter. **241**, 57 (2015).
[10]D. Ikuta, Y. Kono, and G. Shen, "Pressure and temperature dependence of the structure of liquid Sn up to 5.3 GPa and 1373 K," High Press. Res. 1–16 (2016).
[11]Y. Kono, C. Kenney-Benson, C. Park, G. Shen, and Y. Wang, Phys. Rev. B **87**, 24302 (2013).
[12]Y. Kono, C. Kenney-Benson, D. Hummer, H. Ohfuji, C. Park, G. Shen, Y. Wang, A. Kavner, and C. E. Manning, Nat. Commun. **5**, 5091 (2014).
[13]Y. Wang, T. Sakamaki, L. B. Skinner, Z. Jing, T. Yu, Y. Kono, C. Park, G. Shen, M. L. Rivers, and S. R. Sutton, Nat. Commun. **5**, 3241 (2014).
[14]J. M. Besson, R. J. Nelmes, G. Hamel, J. S. Loveday, G. Weill, and S. Hull, Physica B **180–181**, 907 (1992).
[15]Y. Kono, T. Irifune, Y. Higo, T. Inoue, and A. Barnhoorn, Phys. Earth Planet. Inter. **183**, 196 (2010).
[16]R. Kaplow, S. L. Strong, and B. L. Averbach, Phys. Rev. **138**, A1336 (1965).
[17]G. Shen, V. B. Prakapenka, M. L. Rivers, and S. R. Sutton, Rev. Sci. Instrum. **74**, 3021 (2003).
[18]M. J. Assael, K. Kakosimos, R. M. Banish, J. Brillo, I. Egry, R. Brooks, P. N. Quested, K. C. Mills, A. Nagashima, Y. Sato, and W. A. Wakeham, J. Phys. Chem. Ref. Data **35**, 285 (2006).
[19]L. S. Ornstein and F. Zernike, Proc. K. Akad. Van Wet. **17**, 793 (1914).
[20]J. K. Percus and G. J. Yevick, Phys. Rev. **110**, 1 (1958).
[21]N. W. Ashcroft and D. C. Langreth, Phys. Rev. **156**, 685 (1967).
[22]B. R. Orton, Z. Naturforsch. **30a**, 1500 (1975).
[23]E. Canessa, D. F. Mariani, and J. Vignolo, Phys. Status Solidi B **124**, 465 (1984).
[24]X. W. Zou, Z. Z. Jin, and Y. J. Shang, Phys. Status Solidi B **139**, 365 (1987).
[25]N. A. Mauro, J. C. Bendert, A. J. Vogt, J. M. Gewin, and K. F. Kelton, J. Chem. Phys. **135**, 44502 (2011).
[26]J. H. Eggert, G. Weck, P. Loubeyre, and M. Mezouar, Phys. Rev. B **65**, 174105 (2002).
[27]C. Sanloup, J. W. E. Drewitt, C. Crepisson, Y. Kono, C. Park, C. McCammon, L. Hennet, S. Brassamin, and A. Bytchkov, Geochim. Cosmochim. Acta **118**, 118 (2013).
[28]G. Morard, G. Garbarino, D. Antonangeli, D. Andrault, N. Guignot, J. Siebert, M. Roberge, E. Boulard, A. Lincot, A. Denoeud, and S. Petitgirard, High Press. Res. **34**, 9 (2014).
[29]Y. Kono, A. Yamada, Y. Wang, T. Yu, and T. Inoue, Rev. Sci. Instrum. **82**, 23906 (2011).
[30]H. Preston-Thomas, Metrologia **27**, 3 (1990).
[31]A. Hanstrom and P. Lazor, J. Alloys Compd. **305**, 209 (2000).
[32]G. D. Scott and D. M. Kilgour, J. Phys. Appl. Phys. **2**, 863 (1969).
[33]S. Torquato, Phys. Rev. E **51**, 3170 (1995).

Reuse of AIP Publishing content is subject to the terms at: https://publishing.aip.org/authors/rights-and-permissions. Download to IP: 164.54.164.67 On: Mon, 03 Oct 2016 20:30:40